Segregation in binary mixture with differential contraction among active rings

Emanuel F. Teixeira,[1,*] Carine P. Beatrici,[1,†] Heitor C. M. Fernandes,[1,‡] and Leonardo G. Brunnet[1,§]

[1] *Instituto de Física, Universidade Federal do Rio Grande do Sul, CP 15051, CEP 91501-970 Porto Alegre - RS, Brazil*

(Dated: March 6, 2025)

Cell cortex contraction is vital for shaping cells, enabling movement, division, and responding to mechanical signals—processes crucial for multicellular organisms. Differential membrane contractions between cells significantly influence segregation. We present a model where active particle rings interact through differential contraction, showing that segregation arises from this mechanism, with ring activity functioning as an effective temperature. The interface decay exponent is close to $\lambda \sim 1/3$, differing from previous cluster fusion/diffusion model predictions.

In cellular systems made up of different species, sorting is a common emergent behavior. During embryonic development, cells undergo differentiation, which leads to the segregation of cell types in tissue formation. Based on experimental evidence [1–4] and motivated by physical systems like binary mixtures, where spontaneous separation of two liquids is observed, Steinberg proposes [5] that the mechanism for cell segregation lies in the difference in adhesion between cells of different types. This proposal became known as the Differential Adhesion Hypothesis (DAH) or Steinberg Hypothesis.

Harris [6] questions the foundation of the DAH hypothesis, highlighting that maximization of intercellular adhesion does not necessarily lead to the observed effects of cell sorting. He suggested that within a heterogeneous cell aggregate, variation in surface contraction, driven by the active regulation of the acto-myosin cortex, could be the driving force behind tissue engulfment and cell sorting in vivo. The surface contraction of a particular cell appearing more pronounced when it comes into contact with a cell of a different type. Besides that, cells from different tissues exert different surface contraction when contacting the medium. This sorting mechanism was named Differential Surface Contraction Hypothesis (DSCH).

In line with Harris's ideas, Brodland [7] successfully described segregation using finite element simulations that incorporated adhesion and surface contractions, both contributing to the total interfacial tension, a mechanism known as differential interfacial tension hypothesis (DITH). In fact, these hypotheses have been tested using various other extended numerical models, including Cellular Potts [8–13] and Vertex models[14–17]. All theses models define an effective interfacial tension between different units but do not explicitly separate adjacent cell membranes or detail the forces involved, such as adhesion and surface contraction. However, from an experimental perspective, the role of membrane fluctuations was clearly highlighted by Mombach [18], and the distinction between adhesion and cortical tension was emphasized in the work of Krieg et al.[10] and Manning et al. [19].

In this work, we present a model of active rings interacting through differential membrane contraction when within a specific cutoff distance. By utilizing two interacting membranes, this model provides a more detailed representation of biological processes, offering insights into how different layers interact and differentiating the roles of fluctuations, adhesion, and cortex contraction. To our knowledge, this is the first time Harris's mechanism has been simulated in isolation.

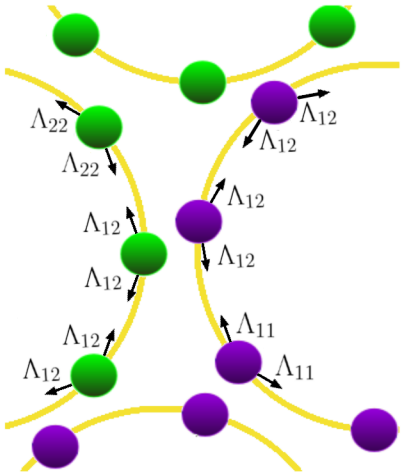

FIG. 1. Active ring model. Contractions occur when two particles from different rings are within a distance l_Λ. The resulting force tends to straighten the membrane.

Boromand and collaborators [20, 21] introduced a ring system composed of passive particles connected by springs. Building on this model, we incorporated active properties into the particles forming the ring in previous articles [22, 23]. We model a 2D system with N rings, each representing a cell formed by n active particles (see Fig. 1). The system is set up as a binary mixture of active rings confined in a circular arena with repulsive walls and radius R_0. The set of coupled overdamped equations governing the dynamics of each particle are: $\dot{\mathbf{r}}_{i,j} = v_0\ \mathbf{n}_j - \mu\,\mathbf{F}_{i,j}$ and $\dot{\mathbf{n}}_j = \sqrt{2\,D_R}\ \boldsymbol{\xi}_j \times \mathbf{n}_j$, where $\mathbf{r}_{i,j}$ denotes the position of the i-th particle within the j-th ring at time t, μ represents its mobility and v_0 is the

magnitude of active velocity with its orientation given by $\mathbf{n}_j$. The second term, $\mathbf{F}_{i,j} = -\boldsymbol{\nabla}_{i,j}E$ represents the total force acting on the i-th particle within the j-th ring. The direction of the active force, described by unit vector $\mathbf{n}_j$, experiences angular Gaussian white noise $\boldsymbol{\xi}_j = \xi_j \hat{e}_z$ with correlation $\langle \xi_j(t_1)\xi_k(t_2)\rangle = \delta_{jk}\delta(t_1 - t_2)$. The noise term D_R represents the rotational diffusion coefficient, which defines a characteristic timescale given by $\tau_R = 1/D_R$.

The energy function has contributions from (i) a perimeter energy (springs connecting ring neighboring particles), (ii) area conservation, (iii) contact-dependent contraction term, (iv) core repulsion among non-neighboring particles from any ring and inter-cellular adhesion,

$$E = \sum_{j=1}^{N} \left\{ \frac{\epsilon_P}{2} \sum_{i=1}^{n} \left(\frac{|\vec{l}_{i,j}|}{l_0} - 1 \right)^2 + \frac{\epsilon_A}{2} \left(\frac{A_j}{A_0} - 1 \right)^2 + \sum_{i=1}^{n} \Lambda_{\alpha\beta} |\vec{l}_{i,j}| \right\} + \frac{\epsilon_c}{2} \sum_{r_{ik} \le \sigma} \left(\frac{r_{ik}}{\sigma} - 1 \right)^2 + \frac{\epsilon_{adh}}{2} \sum_{\sigma < r_{ik} \le l_{adh}} \left(\frac{r_{ik}}{\sigma} - 1 \right)^2, \quad (1)$$

where $\vec{l}_{i,j} = \vec{r}_{i,j} - \vec{r}_{i-1,j}$ is the vector connecting consecutive particles in ring j, ϵ_P is the elastic energy of the spring controlling perimeter fluctuations, and l_0 is the equilibrium distance in the ring. The elastic energy related to area control is ϵ_A, A_j is the inner area of the j-th ring (not considering the area of particles), and A_0 is the equilibrium area. The last two terms in Eq. 1 represent the core repulsion between non-neighboring particles and the adhesion between particles of different rings, respectively. Parameter ϵ_c denotes the characteristic energy of the core repulsion interaction, while r_{ik} is the distance between particles i and k. The equilibrium cut-off distance, σ, effectively defines the particle diameter. The adhesion energy and interaction distance are characterized by ϵ_{adh} and l_{adh}, respectively.

A key distinction between the ring model and other extensive models (Finite Elements [7] and Vertex-Voronoi model [14–17, 24, 25]) lies in the rings contact interface, which comprises two contact membranes. This bring us to the third term in Eq. 1 which incorporates differential surface contraction. In this term, parameter Λ_{11} represents the line tension between particles belonging to type 1 rings (purple rings in Fig. 1), Λ_{22} represents the line tension between type 2 rings and $\Lambda_{12} = \Lambda_{21}$ represents the line tension between rings of different types. All these tensions acting when they are within a cutoff distance l_Λ. A central parameter in this work is $\Lambda = \Lambda_{12}/\bar{\Lambda}$, with $\bar{\Lambda} \equiv (\Lambda_{11} + \Lambda_{22})/2$. We set $\Lambda_{11} = \Lambda_{22} = 0.5$, hence Λ_{12} varies within the range $[0.05 : 5]$.

These tensions result in a force on a ring particle that straightens the interface, acting as an external force on that particle, without affecting its neighbors. Consequently, there is no conservation of momentum for the ring as a whole. Nevertheless, due to the symmetric value of Λ_{ij} ($i = 1, 2;\ j = 1, 2$), the same force will also act on the corresponding particle in the other ring. Therefore, for this particular symmetric case, Newton's third law is applicable to the pair of rings. However, in living systems, interactions aren't always reciprocal [26–29]. Fig. 1 shows a schematic representation of the active ring system, illustrating the involved tensions.

To handle the interaction with the walls, which can be seen as the medium in our context, we specify that the particles of a ring increase their contraction tension once they reach a distance $\sigma/2$ from the wall. This prevents the rings from preferring to accumulate on the wall. The contraction between rings of type 1 (purple) and the "medium" (wall) is defined as $\Lambda_{1M}/\bar{\Lambda} = 12$, while for rings of type 2 (green), we use $\Lambda_{2M}/\bar{\Lambda} = 0$. This choice satisfies the criterion $\Lambda_{12} < \Lambda_{1M} - \Lambda_{2M}$ (valid for all values of Λ_{12} in this work) for the engulfment of one type (purple) by the other (green) [7, 14].

We measure spatial coordinates and time in units of l_0 and τ_R, respectively. As a result, the model equations may be written in terms of the Péclet number [30, 31], defined as $Pe \equiv \frac{v_0 \tau_R}{l_0}$, which controls the level of activity. The system remains in the liquid phase due to the chosen Péclet number ($0.1 < Pe < 0.7$) and shape index $p_0 = \frac{n l_0}{\sqrt{A_0}} = 4$, [20]. Details of the numerical integration method and the remaining parameter values are provided in the Supplemental Material [32].

We begin our simulations with an initial random distribution of rings (see Fig. 2a). For $\Lambda > 1$, we observe a spontaneous segregation process among the rings, with larger Λ values resulting in a smaller interface between ring types, indicating improved segregation. This is illustrated at the bottom of Fig. 2a, where $\Lambda = 10$. (See video 3 in Supplemental Material [32]). For $\Lambda = 1.5$ (middle of Fig. 2a), the system still segregates, but a larger asymptotic interface remains. (See video 2 in Supplemental Material [32]). In contrast, for $\Lambda < 1$ (top of Fig. 2a), an organized mixed state emerges, forming a checkerboard-like pattern where each ring tends to be in contact with a ring of a different type. (See video 1 in Supplemental Material [32]).

To quantify the level of segregation in the system, we use the parameter γ, as introduced by Belmonte and collaborators [33]. This parameter is defined as the mean fraction of neighboring rings of type 2 (green) surrounding rings of type 1 (purple): $\gamma = \left\langle \frac{n_2}{n_1+n_2} \right\rangle_1$, where $\langle .. \rangle_1$ denotes the average over all rings of type 1, with n_1 and n_2 representing the number of first neighbors of type 1 and type 2, respectively. In the literature, it is well established that the segregation parameter is directly correlated with the interface I between the types, expressed as $\gamma \sim I$ [34, 35].

We examined the evolution of the segregation param-

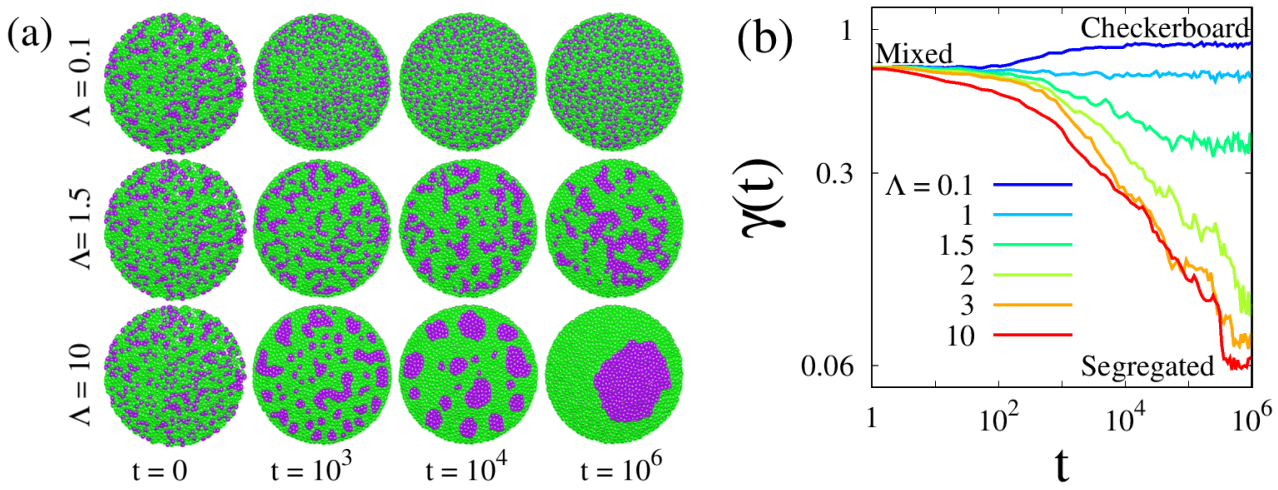

FIG. 2. (a) Snapshots of a binary mixture of rings for various values of Λ. For Λ = 10 (bottom), a stable segregation state emerges, where all clusters eventually merge into a final configuration with a single cluster of the minority type (purple rings). For Λ = 1.5 (center), cluster formation begins but remains unstable, with clusters continuously breaking apart. For Λ = 0.1 (top), system transitions from an initially mixed state to a configuration where rings contact those of a different type, in a checkerboard-like pattern. b) Time series of the segregation parameter for various differential contractions Λ. System begins in a random configuration with 30% purple rings and 70% green rings.

eter γ for various Λ values while keeping the Pe value fixed. As shown in Fig. 2b), the asymptotic value of γ reaches low levels (approximately $\gamma \sim 0.1$ with 10^3 rings) for the segregated state and increases to $\gamma \sim 0.9$ as Λ decreases. The line separating the segregated and checkerboard patterns occurs at $\Lambda \sim 1$, where the initial value of the mixed state ($\gamma \sim 0.7$) is maintained throughout the evolution.

Furthermore, we measured mean values of steady-state γ as a function of Λ for several values of Pe (see Fig. 3a). Here we emphasize the role of parameter Pe, which broadens the transition as its value increases, and the importance of initial configurations to avoid stay trapped in a meta-stable state. While at low Pe values ($Pe \leq 0.2$ in Fig. 3a) and $\Lambda < 1$, the system evolves to the checkerboard pattern, for $\Lambda > 1$ it remains trapped close to the initial configuration, so we employed the segregated state as the initial condition to test the effect of Pe. In brief, Pe functions like temperature, enabling the system to overcome potential barriers to approach the minimum energy state. Simultaneously, it is responsible for deviating from the optimal value due to the introduced fluctuations.

In Fig. 3b we present a ($\Lambda \times Pe$) diagram, colors indicate the mean value for γ. At low Pe values, the segregation region occurs just above $\Lambda = 1$, but at high activity we observe a mixed state well above this limit. This indicates that the segregation criterion [7, 14] $\Lambda_{12} > (\Lambda_{11} + \Lambda_{22})/2$ is only valid at low Pe. Similar arguments apply to the checkerboard state in the region defined by $\Lambda < 1$.

Additionally, we conducted an analysis similar to pre-

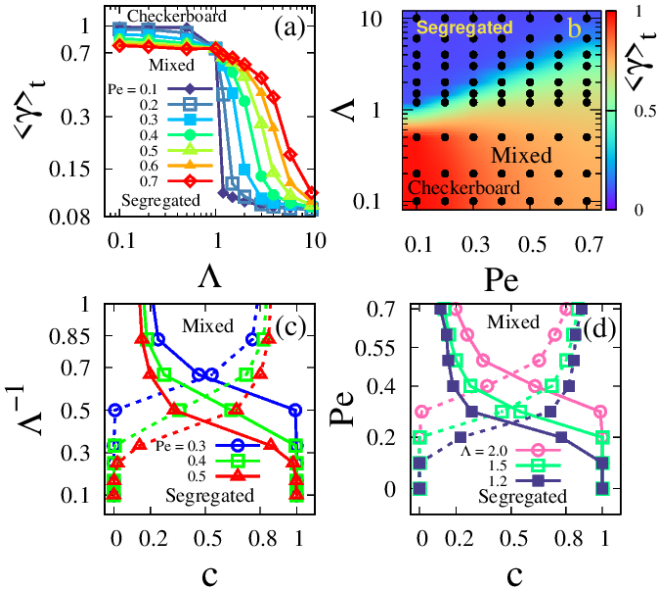

FIG. 3. (a) Steady-state mean values of segregation parameter γ as a function of Λ for various values of Pe. (b) Diagram ($Pe \times \Lambda$) that separates checkerboard, mixed and segregated regions. Colors represent the average values of segregation parameter for long times. (c) Binodal curves from the concentration c of rings of type 1 (purple ones) inside the largest cluster c_{in} and outside c_{out} (dashed lines) for three values of Pe. See text for details. (d) Binodal curves from the concentration c of rings of type 1 (purple ones) inside the largest mean cluster c_{in} and outside c_{out} (dashed lines) for three values of Λ. See text for details. Fixed parameter: $N = 500$.

vious works [36] and observed how the steady state of largest cluster of type 1 rings (purple) changes with Pe

and Λ. We define the fraction of these rings that are inside the largest cluster as $c_{in} = N_{int}/N_1$. N_1 and N_{int} are the total number of type 1 rings and the number of rings in the largest asymptotic cluster, correspondingly. Using $c_{out} = 1 - c_{in}$, we can construct a binodal curve that delineates regions of segregation and mixing as function of Λ^{-1} and Pe (see Figures 3c-d). Below the intersection we have the segregated state ($c_{in} \sim 1$ and $c_{out} \sim 0$, one large cluster) and above, the mixed state (several clusters of similar size). Fig. 3d shows the effect of the activity parameter Pe on the binodal curves. Depending on the value of Λ, there is a value of Pe beyond which the system transitions from segregated to mixed state.

Our focus now shifts to understanding how the system evolves from a randomly mixed configuration to a segregated one. This is particularly important because the long time behavior before saturation of the segregation parameter and the mean size growth of clusters can provide information about the underlying mechanisms occurring during tissue formation. The mean cluster's size of rings of type 1, $M(t)$, is obtained using the cluster-counting algorithm used by Beatrici et al. [34]. Here, we analyze the case where contact between different rings type is unfavorable ($\Lambda = 10$). Initially, the system is in a mixed configuration with a corresponding value of $\gamma \equiv \gamma_0 = 0.7$, consequent of the (30:70) proportion of ring types. In Fig. 4a, we show the evolution of the segregation parameter normalized by its initial value, $\bar{\gamma}(t) = \gamma(t)/\gamma_0$. The activity Pe determines the duration of the transient period, with higher activity implying shorter transients. Subsequently we observe an algebric decay, $\gamma \sim t^{\lambda}$ with an exponent close to $-1/3$ for at least two decades, independent of the activity value Pe. Additionally, in this regime, the mean domain size M grows with an exponent close to $2/3$ (see Fig. 4c). Thus, we observe an inverse relationship, $\gamma \sim M^{-2}$, consistent with previous findings [11, 13, 17, 35].

In Fig. 4b, we observe that significantly unequal proportions slow down the domain growth process, as it relies on the coalescence of minority clusters diffusing within the majority type.(See video 4 in Supplemental Material [32]). However, when the proportions are equal (50:50), the dynamics change — the system quickly percolates, and the process of interface reduction becomes dominated by rounding. In this case, we expect exponent $\sim -1/2$ [37]. For other proportions, we observe asymptotic time exponents close to $-1/3$ and $2/3$ for γ and M, respectively, while maintaining the inverse relationship, $\gamma \sim M^{-2}$ (see Fig. 4b-d).

In conclusion, we present a model where cells are represented by rings of active particles. Each ring being explicitly equipped with its own membrane, allowing it to accommodate negative curvatures and replicate all cell sorting mechanisms, whether in isolation or combined. This represents a significant advancement in the class of extended cell models, offering a path to more realistic depiction of cell behavior as observed in experiments.

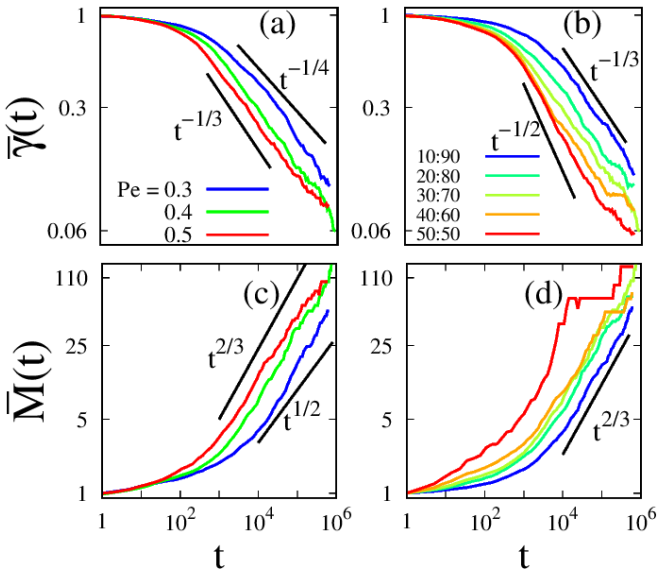

FIG. 4. (a) Evolution of the rescaled segregation parameter $\bar{\gamma}(t) = \gamma(t)/\gamma_0$ and (c) mean cluster size $\bar{M}(t) = M(t)/M_0$ for different values of Pe. Ring type ratio: 30:70. (b) Temporal evolution of the rescaled segregation parameter $\bar{\gamma}(t)$ and (d) mean cluster size $\bar{M}(t)$ for different ratios of ring types. The activity level is $Pe = 0.4$. The number of rings and the tension in all cases is $N = 10^4$ and $\Lambda = 10$, respectively.

By employing this comprehensive cellular model and incorporating a term for differential contraction among rings of different types, we conducted a numerical evaluation of Harris' proposed hypothesis on cellular differential surface contraction [6]. We observed a monotonic relationship between the differential contraction parameter Λ and the steady-state segregation parameter $\langle\gamma\rangle_t$, showing a tendency toward segregation for $\Lambda > 1$ and a checkerboard pattern for $\Lambda < 1$. We found that by keeping all cells with identical attraction forces and solely employing adequate differential interfacial contraction the system segregates. The differences in ring areas are minimal, which rules this out as a potential segregation mechanism [38]. (See Supplementary Material [32]). Mechanisms such as motility-induced phase separation (MIPS) are also dismissed since the Péclet values used here ($Pe \leq 0.7$) are well below the range where this transition occurs [39–41].

The rate at which the system transitions from an initially mixed state to its asymptotic state, as well as the ultimate value it reaches, also depends on the activity level Pe. In the case of segregation ($\Lambda > 1$), increased activity has a tendency to disrupt the configuration of minimum interfacial energy. Binodal curves, showing a transition between the mixed and the segregated states, corroborate the inverse correlation between the contraction interaction Λ and the activity Pe. These findings suggest that the activity Pe plays a role similar to temperature

in thermodynamic equilibrium systems [30, 31, 42].

Furthermore, we found that the segregation parameter $\gamma(t)$ and the mean cluster size $M(t)$ exhibit a power-law regime with an exponent close to $-1/3$ and $2/3$, respectively. The activity Pe changes the typical timescale at which the asymptotic regime begins but does not modify the growth exponent of the domains. Similarly, the proportions do not alter the characteristic exponent, except in the (50:50) case where the system starts close to percolation and the evolution appears to be dominated by rounding. We observed an inverse relationship between the segregation parameter and the typical size, $\gamma \sim M^{-2}$.

Finally, the observed segregation exponent of $\lambda = -1/3$ is at odds with the literature. The cluster-cluster aggregation mechanism seen in our simulations would typically correspond to an exponent of $\lambda = -1/4$, as predicted by surface diffusion models [43, 44] or mean cluster models [45, 46], particularly in the absence of alignment interactions. An exponent of $\lambda = -1/3$ would instead be expected from the Cahn-Hilliard equation if the mechanism were evaporation-condensation, which we do not observe. The reasons for these discrepancies will be explored in future studies.

We express our gratitude to the Brazilian agencies CAPES, CNPq, and FAPERGS for their financial support. H.C.M.F. and L.G.B. acknowledge the support from the National Council for Scientific and Technological Development – CNPq (procs. 402487/2023-0 and 443517/2023-1). E.F.T. acknowledges ICTP-SAIFR/IFT-UNESP. The simulations were conducted using the VD Lab cluster infrastructure at IF-UFRGS. This work is dedicated to the memory of Albert Kenneth Harris Jr.

* emanuel.teixeira@ufrgs.br
† carine@if.ufrgs.br
‡ heitor.fernandes@ufrgs.br
§ leon@if.ufrgs.br

[1] R. G. Harrison, Journal of Experimental Zoology **9**, 787 (1910).
[2] A. Moscona, Experimental Cell Research **3**, 535 (1952).
[3] J. P. Trinkaus and P. W. Groves, Proceedings of the National Academy of Sciences **41**, 787 (1955).
[4] P. Weiss and A. Taylor, Proceedings of the National Academy of Sciences **46**, 1177 (1960).
[5] M. S. Steinberg, Science **141**, 401 (1963).
[6] A. K. Harris, Journal of Theoretical Biology **61**, 267 (1976).
[7] G. W. Brodland, J. Biomech. Eng. **124**, 188 (2002).
[8] F. Graner and J. A. Glazier, Physical review letters **69**, 2013 (1992).
[9] J. Käfer, T. Hayashi, A. F. Marée, R. W. Carthew, and F. Graner, Proceedings of the National Academy of Sciences **104**, 18549 (2007).
[10] M. Krieg, Y. Arboleda-Estudillo, P.-H. Puech, J. Käfer, F. Graner, D. Müller, and C.-P. Heisenberg, Nature cell biology **10**, 429 (2008).
[11] A. Nakajima and S. Ishihara, New Journal of Physics **13**, 033035 (2011).
[12] L. Canty, E. Zarour, L. Kashkooli, P. François, and F. Fagotto, Nature communications **8**, 157 (2017).
[13] M. Durand, PLOS Computational Biology **17**, e1008576 (2021).
[14] D. L. Barton, S. Henkes, C. J. Weijer, and R. Sknepnek, PLOS Computational Biology **13**, 1 (2017).
[15] D. M. Sussman, J. Schwarz, M. C. Marchetti, and M. L. Manning, Physical review letters **120**, 058001 (2018).
[16] H. B. Wolff, L. A. Davidson, and R. M. Merks, Bulletin of Mathematical Biology **81**, 3322 (2019).
[17] M. Krajnc, Soft Matter **16**, 3209 (2020).
[18] J. C. M. Mombach, J. A. Glazier, R. C. Raphael, and M. Zajac, Phys. Rev. Lett. **75**, 2244 (1995).
[19] M. L. Manning, R. A. Foty, M. S. Steinberg, and E.-M. Schoetz, Proc Natl Acad Sci U S A **107**, 12517 (2010).
[20] A. Boromand, A. Signoriello, F. Ye, C. S. O'Hern, and M. D. Shattuck, Physical Review Letters **121**, 248003 (2018).
[21] J. D. Treado, D. Wang, A. Boromand, M. P. Murrell, M. D. Shattuck, and C. S. O'Hern, Physical Review Materials **5**, 055605 (2021).
[22] E. F. Teixeira, H. C. Fernandes, and L. G. Brunnet, Soft Matter **17**, 5991 (2021).
[23] G. Ourique, E. Teixeira, and L. Brunnet, Physica A: Statistical Mechanics and its Applications **589**, 126661 (2022).
[24] D. Bi, J. Lopez, J. M. Schwarz, and M. L. Manning, Nature Physics **11**, 1074 (2015).
[25] D. Bi, X. Yang, M. C. Marchetti, and M. L. Manning, Physical Review X **6**, 021011 (2016).
[26] B. Bhattacherjee, M. Hayakawa, and T. Shibata, Soft Matter **20**, 2739 (2024).
[27] T. Hiraiwa, Phys. Rev. Lett. **125**, 268104 (2020).
[28] J. LaChance, K. Suh, J. Clausen, and D. J. Cohen, PLoS computational biology **18**, e1009293 (2022).
[29] H. Yamanaka and S. Kondo, Proceedings of the National Academy of Sciences **111**, 1867 (2014).
[30] Y. Fily and M. C. Marchetti, Physical review letters **108**, 235702 (2012).
[31] Y. Fily, S. Henkes, and M. C. Marchetti, Soft matter **10**, 2132 (2014).
[32] See Supplemental Material at [URL will be inserted by publisher] for videos and simulation details, which includes Refs. [14, 17, 20, 24, 25, 38].
[33] J. M. Belmonte, G. L. Thomas, L. G. Brunnet, R. M. C. de Almeida, and H. Chaté, Phys. Rev. Lett. **100**, 248702 (2008).
[34] C. P. Beatrici, R. M. C. de Almeida, and L. G. Brunnet, Phys. Rev. E **95**, 032402 (2017).
[35] F. Franke, S. Aland, H.-J. Böhme, A. Voss-Böhme, and S. Lange, PLoS computational biology **18**, e1010460 (2022).
[36] S. N. Weber, C. A. Weber, and E. Frey, Physical review letters **116**, 058301 (2016).
[37] J.-P. Rieu and Y. Sawada, The European Physical Journal B - Condensed Matter and Complex Systems **27**, 167 (2002).
[38] X. Yang, M. L. Manning, and M. C. Marchetti, Soft matter **10**, 6477 (2014).
[39] Y. Fily and M. C. Marchetti, Phys. Rev. Lett. **108**, 235702 (2012).

[40] G. S. Redner, M. F. Hagan, and A. Baskaran, Biophysical Journal **104**, 640a (2013).
[41] M. E. Cates and J. Tailleur, Annu. Rev. Condens. Matter Phys. **6**, 219 (2015).
[42] C. Bechinger, R. Di Leonardo, H. Löwen, C. Reichhardt, G. Volpe, and G. Volpe, Reviews of modern physics **88**, 045006 (2016).
[43] A. Sicilia, Y. Sarrazin, J. J. Arenzon, A. J. Bray, and L. F. Cugliandolo, Phys. Rev. E **80**, 031121 (2009).
[44] J. W. Cahn and J. E. Hilliard, The Journal of chemical physics **28**, 258 (1958).
[45] C. P. Beatrici, R. M. de Almeida, and L. G. Brunnet, Physical Review E **95**, 032402 (2017).
[46] M. Kolb, Phys. Rev. Lett. **53**, 1653 (1984).